Materials Advances

ROYAL SOCIETY OF CHEMISTRY

PAPER

View Article Online
View Journal | View Issue

Cite this: *Mater. Adv.*, 2022, 3, 5796

Photocatalytic dye degradation using $BiVO_4$–paint composite coatings†

Manish Kumar and Rahul Vaish *

Received 19th March 2022,
Accepted 24th May 2022

DOI: 10.1039/d2ma00316c

rsc.li/materials-advances

Bismuth vanadate ($BiVO_4$)–paint composites coated on the aluminium sheet surface were fabricated with different $BiVO_4$ amounts (0, 20, and 40 wt%) in paint. The degradation capability of the methylene blue (MB) dye using the $BiVO_4$–paint coated sample was explored. The impact of $BiVO_4$ content on the dye degradation performance was analyzed. The fabricated materials were characterized using scanning electron microscopy (SEM) and X-ray diffraction (XRD). XRD confirmed the existence of the $BiVO_4$ crystalline phase in paint. The elemental composition of the sample was determined using X-ray electron diffraction spectroscopy (EDS) inbuilt in SEM. The absorption spectra of $BiVO_4$ was determined using an UV-Vis-NIR spectrophotometer. As the content of $BiVO_4$ in the $BiVO_4$–paint sample increases, there is an increase in the dye degradation efficiency. The 40 wt%-$BiVO_4$–paint sample exhibited an ~72% dye degradation efficiency as compared to the 0 wt%-$BiVO_4$–paint sample (~27%) in a duration of 240 min of the photocatalysis experiment. The photocatalytic MB dye degradation is in accordance with the pseudo-first-order kinetics attaining the largest k value of 0.00524 min^{-1}. Photocatalytically treated water after the photocatalysis experiment falls in the moderate phytotoxicity level. A germination index study was done using *Vigna radiata* seeds.

1. Introduction

Clean and safe water is considered one of the most essential natural resources for the survival of living beings on earth.[1,2] Due to rapid urbanization, there incurred an increase in water contamination due to effluents discharged directly to water bodies.[3] Moreover, industries such as textile, pharmaceuticals, mining, *etc.* also discharge polluted water in enormous quantities directly to the environment.[4] The release of dyes from the textile industry directly into the environment is a concern. Dyes are harmful pollutants for living beings because of their toxic and carcinogenic nature.[5] So, getting safe water is a global concern at present. In this regard, various water treatment methods such as biological, physical, and chemical processes have been adopted to overcome these issues.[6–10] The recalcitrant nature of a few pollutants limits the use of biological treatment processes,[11,12] and at the same time chlorination, ozonation and high cost retard the usage of chemical processes for water treatment.[12,13] Physical techniques including coagulation, absorption, ion exchange, and ultrafiltration cause secondary pollutant byproducts or simply transfer pollutants from one phase to another. So this may cause an increase in cost for further treatment processes.[14–16] Photocatalysis is considered one of the efficient water treatment processes in recent years owing to its several advantages such as no waste byproducts, environmental friendliness, low cost, and complete mineralization.[17–19] When the surface of a semiconductor photocatalyst material absorbs photon energy, there is the generation of electrons in the conduction band (CB) and holes in the valence band (VB). These generated electrons and holes further react with the water molecules generating highly active superoxide and hydroxyl radicals which further degrade the organic pollutants present in the contaminated water to carbon dioxide and water as end products.[20,21] In recent years, several photocatalyst materials such as TiO_2, ZnO, $BiVO_4$, WO_3, ZnS, CeO_2, *etc.* have been reported.[22–25] TiO_2 displays excellent photocatalytic activity but its usage is restricted due to its wide bandgap (3.2 eV) which needs ultraviolet (UV) light as a source for activation.[26] ZnO has a bandgap of 3.37 eV, the usage of which is limited by UV light irradiation.[27,28] Visible light occupies ~45% of solar light, while UV light occupies ~3–5%.[29] This led to the search for new photocatalytic materials that can be visible light active. In this context, $BiVO_4$ would be a better option as a photocatalyst as it possesses the unique property of a narrow bandgap (2.4 eV), corrosion resistance, non-toxicity, stability, and good dispersibility.[30–34] Based on density functional theory (DFT) calculations, researchers have claimed that the VB of monoclinic bismuth vanadate (m-$BiVO_4$) constitutes Bi-6s and O-2p orbitals, while the CB constitutes

School of Engineering, Indian Institute of Technology Mandi, Mandi, Himachal Pradesh, 175005, India. E-mail: rahul@iitmandi.ac.in

† Electronic supplementary information (ESI) available. See DOI: https://doi.org/10.1039/d2ma00316c

V-3d orbitals.[35–37] In the monoclinic scheelite structure, the 6s state of Bi^{3+} is situated above the O-2p orbital, resulting in reduced bandgap and viable transition from Bi-$6s^2$ to V-3d. Walsh *et al.* used DFT calculations to demonstrate that hybridization among Bi-6s and O-2p states at the apex of the VB is the reason for the reduced bandgap for m-$BiVO_4$. It showed that $BiVO_4$ possesses a direct bandgap.[38] The monoclinic scheelite structure is reported to give the best visible light photocatalytic degradation.[39] $BiVO_4$ can be synthesized through the hydrothermal method, microwave-assisted methods, co-precipitation, solid-state synthesis, and sono-chemical method.[40–43]

Paints are considered one of the important construction materials among steel, window glass, cement, insulation materials, *etc.* Engineered material usage is encouraged to improve existing conventional products or to improve or create products with new functions and applications. SiO_2, Fe_2O_3, Al_2O_3, carbon-nanotubes (CNTs), and ZrO_2 have been utilized to enhance the longevity and quality of structures.[44,45] Incorporating materials such as Ag, CNTs, SiO_2, ZnO, CeO_2, Fe_2O_3, and TiO_2 in paints can enhance properties like easy cleaning, UV-protection, scratch resistance, anti-corrosion, antibacterial activity, fire resistance, and wood preservation.[46–49] Paints are applied to protect substrates from environmental effects and for appealing needs. It is an economical way to safeguard metals from getting corroded compared to other surface protection methods.[50] Coatings are applied as thin layers over substrates like metals and wood as a protection against corrosion and for decoration.[51] Incorporating different materials into paints have been reported to improve their UV resistance,[52] rheological properties,[53] coloring,[54] and mechanical properties (SiO_2).[55] Paints consist of different components like binders, pigments, solvents, fillers, diluents, and several additives such as thickeners, antifoam agents, and dispersing additives.[56] TiO_2 embedded in paint has been reported to induce a photocatalytic effect for reducing nitrogen oxides and volatile organic compounds present as air pollutants in the environment.[57–60] Photocatalytic paints have self-cleaning properties since they tend to remove unwanted substances from the surface using the photon energy of light.[61] Paints usually use pigments such as TiO_2 which are photocatalytically inactive, suppressing the possibility of photo-oxidization of the polymer binder, thereby causing photochalking. The paint pigments comprise non-active rutile titania particles which are surface-treated with silica or alumina, ensuring photocatalytic passivity. Such pigments stabilize paints to be used as an exterior coating, thereby blocking solar UV radiation.[62,63] Baudys *et al.* have suggested exposing the sample containing acrylate or silicate binders for a certain weathering time, causing degradation of the polymer binder, and at the same time would unblock the photocatalyst surface to avail better photocatalytic activity. The stability of the polymer binder should be analyzed to obtain paints with photocatalytic activity and a reasonable lifetime.[63] Islam *et al.* have recently reported a photocatalytic paint based on a photopolymer resin and TiO_2 for degrading organic pollutants in water.[64] Bonnefond *et al.* have reported stable photocatalytic paints incorporating TiO_2 and an acrylic polymer for bacterial disinfection.[65,66] Microspheres of TiO_2 incorporated in acrylic paints have been reported for photocatalytic methylene blue (MB) dye degradation.[67] Only a few reports are available regarding photocatalytic coatings and paints. Research on the use of paints for photocatalysis has not been much explored, which needs further investigation.

In this study, we intend to explore a photocatalyst material that can be visible light active, economical, and free from the quest to recover the catalyst and at the same time the support utilized should possess corrosion, abrasion, and acidic particle resistance. The simple preparation method, possibility of large-scale applicability on various substrates, and being devoid of hazardous chemicals and no need for the use of sophisticated instruments make this study remarkable. We explored MB dye degradation in visible light using $BiVO_4$–paint composites coated on a rectangular aluminium sheet where the aluminium sheet acts as a support/substrate. Adhesion of paints incorporated with $BiVO_4$ over the surface of the aluminium sheet as a coating is easy.[68] The photocatalyst will be used in wastewater so corrosion of the substrate needs consideration. Aluminium is known to possess high anti-corrosion properties, abrasion resistance, and acidic particle resistance, so it has been selected as the substrate.[69,70] Paint is a commonly used construction material and can also adhere to the substrate easily so it can be considered as an ideal material to load the photocatalyst. The usage of a paint-coated substrate for wastewater remediation through the photocatalysis experiment using visible light irradiation would be both economical as well as free from separation and filtration processes to recover the catalyst. The $BiVO_4$–paint composite coated on an aluminium substrate for photocatalytic MB dye degradation has not been explored so far.

2. Materials and methods

2.1 Fabrication of $BiVO_4$

Oxide powders of Bi_2O_3 and V_2O_5 in a stoichiometric molar ratio were homogeneously mixed manually through the use of an agate mortar pestle for approximately 30 minutes. Once the powders were homogeneously mixed, the mixture was subjected to calcination at 700 °C for 8 hours by placing in a furnace to get the pure $BiVO_4$ (BiV) phase.

2.2 Fabrication of BiV-paint

BiV-paint samples were prepared by coating the catalyst on the rectangular aluminium sheet as shown in Scheme 1. The dimensions of the aluminium substrate used were 20 mm × 20 mm × 1 mm. The aluminium substrate was cleaned with distilled (DI) water and acetone thrice to eradicate any contamination present over its surface. Berger Luxol high gloss enamel paint was used as a coat on the substrate. For fabrication of the BiV-paint sample, $BiVO_4$ and paint were mixed to form a slurry, where 0%, 20 wt%, and 40 wt% of $BiVO_4$ was added to the paint. Here the calculation for the coating was done for 0.8 g in which specified wt% of the $BiVO_4$ catalyst was mixed. The slurry

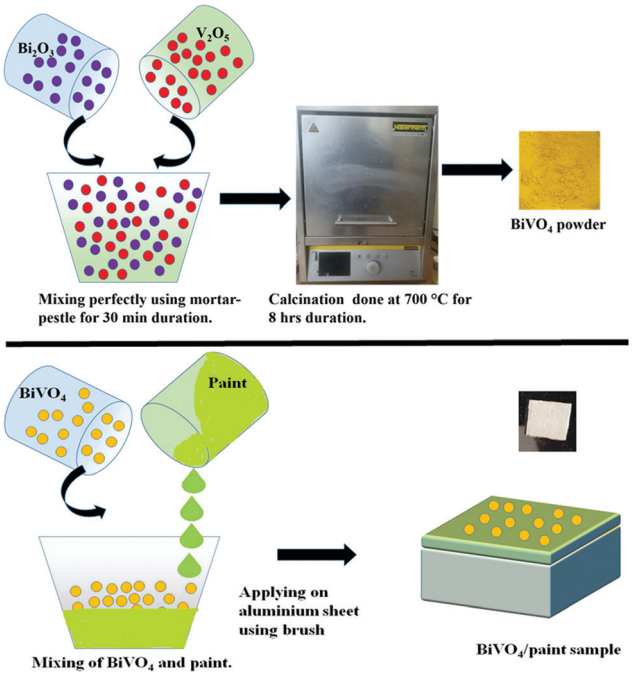

Scheme 1 Schematic illustration showing the synthesis method adopted for BiV-paint.

was hand-mixed for approx. 10 minutes to obtain a homogenous mixture using a brush. The slurry of $BiVO_4$ and paint was then applied on both sides of the rectangular aluminium sheets using a brush in order to obtain a uniform coating. The coated sample was covered and kept safely for drying in the environment for 5 days. The obtained dried samples with 0%, 20 wt%, and 40 wt% were named paint, 20BiV-paint, and 40BiV-paint, respectively.

2.3 Characterization of BiV-paint

The crystalline structural analysis of the prepared $BiVO_4$–paint composite was conducted using an X-ray diffractometer (XRD) (Rigaku, Japan (9 kW Cu-Kα anode)). The sample was scanned at 3° min^{-1} over the 10–80° range. The surface morphology and microstructures of the paint sample were analyzed using a Nova Nano SEM-450 field emission scanning electron microscope (FE-SEM). The elemental chemical composition of the sample was analyzed using X-ray electron diffraction spectroscopy (EDS) which is inbuilt in SEM. The photoluminescence spectra of the samples were recorded using a LabRAM HR Evolution photoluminescence spectrometer (HORIBA, Japan) in the scan range of 350 to 650 nm. An excitation wavelength of 325 nm was used to record the spectra. The absorption spectra of $BiVO_4$ were determined using a UV-Vis-NIR spectrophotometer (Shimadzu UV-3150a).

2.4 Photocatalytic experiment

Each of the obtained paint, 20BiV-paint, and 40BiV-paint samples was utilized to degrade MB dye solution under visible light illumination with the use of 2 Havells bulbs (15 W each). Further, 0.11 g of $BiVO_4$ powder was subjected to the photocatalysis experiment and its degradation capability was analyzed. Prior to the start of the experiment, it was made sure to achieve adsorption–desorption saturation for the MB dye and the samples by employing continuous stirring (500 rpm) in a dark environment. On the attainment of the adsorption saturation, the used dye was replaced with a fresh 10 ml dye with an initial concentration of ~5 mg L^{-1}. After finishing 30 min of the photocatalysis experiment, each time a 1 mL solution was taken from the beaker in order to quantify the dye degradation, and on completion of the quantification, it was replenished back to the beaker so as to sustain the constant volume of dye in the beaker. The dye removal percentage was analyzed using eqn (1):[71]

$$\%\text{removal of MB dye} = \frac{C_o - C}{C_o} \times 100 \quad (1)$$

where C_o and C denote the initial dye concentration and that obtained after time duration 't', respectively.

Diffuse reflectance spectroscopy (DRS) was conducted to obtain the absorption spectra of the $BiVO_4$ powder which was further transformed into Tauc plots (plot of $(\alpha E)^2$ *vs.* E) to obtain a direct band gap.[72,73]

2.5 Phytotoxicity test

Distilled (DI) water and sample water collected after 0 and 4 h of photocatalysis were used to conduct seed germination and root length tests. This test determines the sustainability and suitability of the degraded MB dye water post photocatalysis for seed (*Vigna radiata*) germination. This would help in understanding the reuse of the collected water after the photocatalysis experiment. For testing, 3 vials each containing 10 seeds of *Vigna radiata* were taken. The vials were sprinkled everyday with 0.5 ml of treated, untreated, and DI water. The test was conducted in Mandi, India where the environmental temperature was 25 °C. The results were analyzed 7 days after the test. The evaluation of the outcome was done after completion of the duration of 7 days. AFNOR ISO 17126 was followed to determine the root length and seed germination counts.[74] The germination index was evaluated using eqn (2):[75]

$$\text{GI}(\%) = \frac{\text{Seed germination (\%)} \times \text{root length of treatment}}{\text{Seed germination (\%)} \times \text{root length of control}} \times 100 \quad (2)$$

3. Results and discussion

Fig. 1 presents the XRD plots of the BiV, paint, 20BiV-paint, and 40BiV-paint samples. The prepared samples are of a high crystalline quality which can be observed through the presence of sharp XRD peaks. The BiV, 20BiV-paint, and 40BiV-paint samples demonstrate very good agreement with the pure monoclinic phase of $BiVO_4$ following the standard reference JCPDS 01-075-1866. The XRD results indicate the complete phase formation of the $BiVO_4$ powder sample. All the major peaks of $BiVO_4$ can be easily identified in 20BiV-paint and

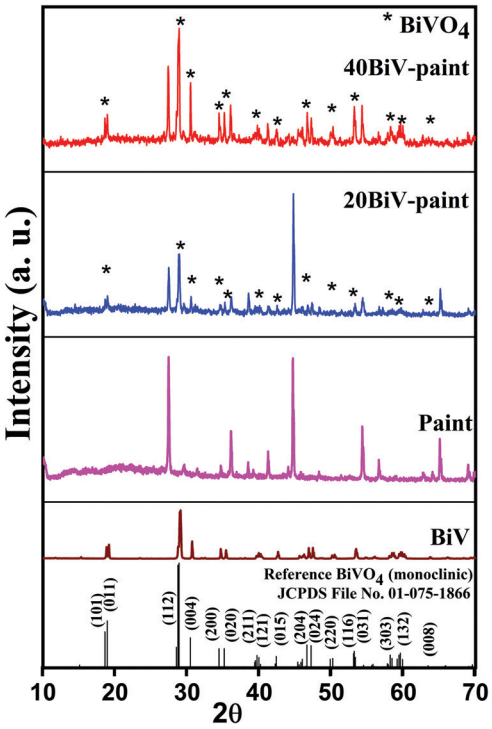

Fig. 1 XRD plots of BiV, paint, 20BiV-paint, and 40BiV-paint samples.

40BiV-paint samples. The presence of additional peaks in 20BiV-paint and 40BiV-paint samples is due to other constituents of the paint. Paint may possess many metal oxides such as Al_2O_3, SiO_2, CaO, TiO_2, *etc.*[76] As the exact constituents of paints are not readily available, unknown peaks have not been identified.

The SEM images of $BiVO_4$, paint, and 40BiV-paint were taken to demonstrate their surface morphology as shown in Fig. 2(a–c). Fig. 2(a) demonstrates the irregular shape morphology of the $BiVO_4$ particles. Fig. 2(b and c) demonstrate the microstructures of the paint and 40BiV-paint samples. The presence of Bi, V, and O along with other elements in 40BiV-paint can be observed through the EDS elemental color map as shown in Fig. 2(d and e). The EDS spectrum shown in Fig. 2(f) confirms the presence of C, O, Al, Si, Bi, V, Ca, and Ti elements in the 40BiV-paint sample.

In order to determine the applicability of $BiVO_4$ powder for the photocatalysis experiment in visible light, the DRS spectrum of the $BiVO_4$ powder sample was recorded. The adsorption edge of the BiV powder and its explored bandgap (2.42 eV) are displayed in Fig. 3(a) and (b), respectively. The absorption edges of 40BiV-paint and paint are shown in the inset of Fig. 3(a). The inset of Fig. 3(b) shows the explored bandgaps of 40BiV-paint and paint as 2.1 eV and 2.07 eV, respectively. Paint may constitute many different elements so its bandgap value is low. The obtained bandgap lies in the visible region so this affirms that BiV powder is suitable for photocatalytic dye degradation experiments in visible light.

Fig. 4 shows the recorded photoluminescence spectra of BiV, 40BiV-paint, and paint using an excitation wavelength of 325 nm. A high PL intensity denotes a higher rate of electron–hole pair recombination.[77] A lower PL intensity value indicates that there exists a higher electron transfer efficiency which increases the degradation of contaminants and thus enhances the photocatalytic efficiency.[78,79] It can be seen that there is a gradual decrease in the PL intensity. The PL intensity of 40BiV-paint is lower than that of paint which suggests that electron–hole pair recombination is suppressed in the case of 40BiV-paint. A very low PL intensity of $BiVO_4$ may be due to the formation of structural defects during calcination which traps the electrons.[80] This can be viewed in the PL spectra of BiV.

The obtained BiV powder was used as a catalyst for degrading MB dye through the photocatalysis experiment and the obtained results are shown in Fig. 5(a). Prior to the start of the photocatalysis experiment, it was made sure that adsorption saturation was attained carefully. Fig. 5(a) reveals that as the irradiation time is elevated there occurs a substantial decrease in the peak intensity of the MB dye, which affirms the degradation of the MB dye. Fig. 5(b) shows the $\frac{C}{C_o}$ *vs.* time plots attained with and without sample usage during the photocatalysis experiment. According to the results, without sample use (control) ~27% dye degradation is attained in 240 min, while with BiV powder usage the attained degradation percentage raises to ~53% within 240 min of visible light illumination. There is a 26% more degradation efficiency of MB dye as compared to that of the control sample. This approves the good photocatalytic ability of $BiVO_4$.

The obtained 40BiV-paint sample was used as a catalyst for degrading MB dye through the photocatalysis experiment and the obtained results are shown in Fig. 6(a). Fig. 6(a) shows that as the irradiation time is elevated there occurs a substantial decrease in the peak intensity of the MB dye, which affirms MB dye degradation. Fig. 6(b) displays the $\frac{C}{C_o}$ *vs.* time plots attained with paint, 20BiV-paint, and 40BiV-paint and without sample usage during the photocatalysis experiment. The degradation efficiency attained without the use of the sample (control) is ~27%, while with the use of paint, 20BiV-paint, and 40BiV-paint samples it raises to 50%, 67%, and 72%, respectively, in 240 minutes of visible light irradiation. Here, 20BiV-paint and 40BiV-paint samples attain improvements of 40% and 45%, respectively, in the degradation efficiency as compared to that attained by the control sample. The crystalline peaks in the paints would have contributed to attain 23% more degradation of the dye than the control sample. Improvements of 17% and 22% attained by 20BiV-paint and 40BiV-paint samples, respectively, would be due to the $BiVO_4$ catalyst loading. Fig. 6(c) shows the $\frac{C}{C_o}$ *vs.* time plots for different MB dye concentrations (5, 10, and 12.5 mg L^{-1}). In order to know the active radicals present during the photocatalysis experiment, isopropanol (IPA), ethylenediaminetetraacetic acid (EDTA), and *p*-benzoquinone (*p*-BQ) scavengers were appended individually in the MB dye solution with a view to seize the different active radicals

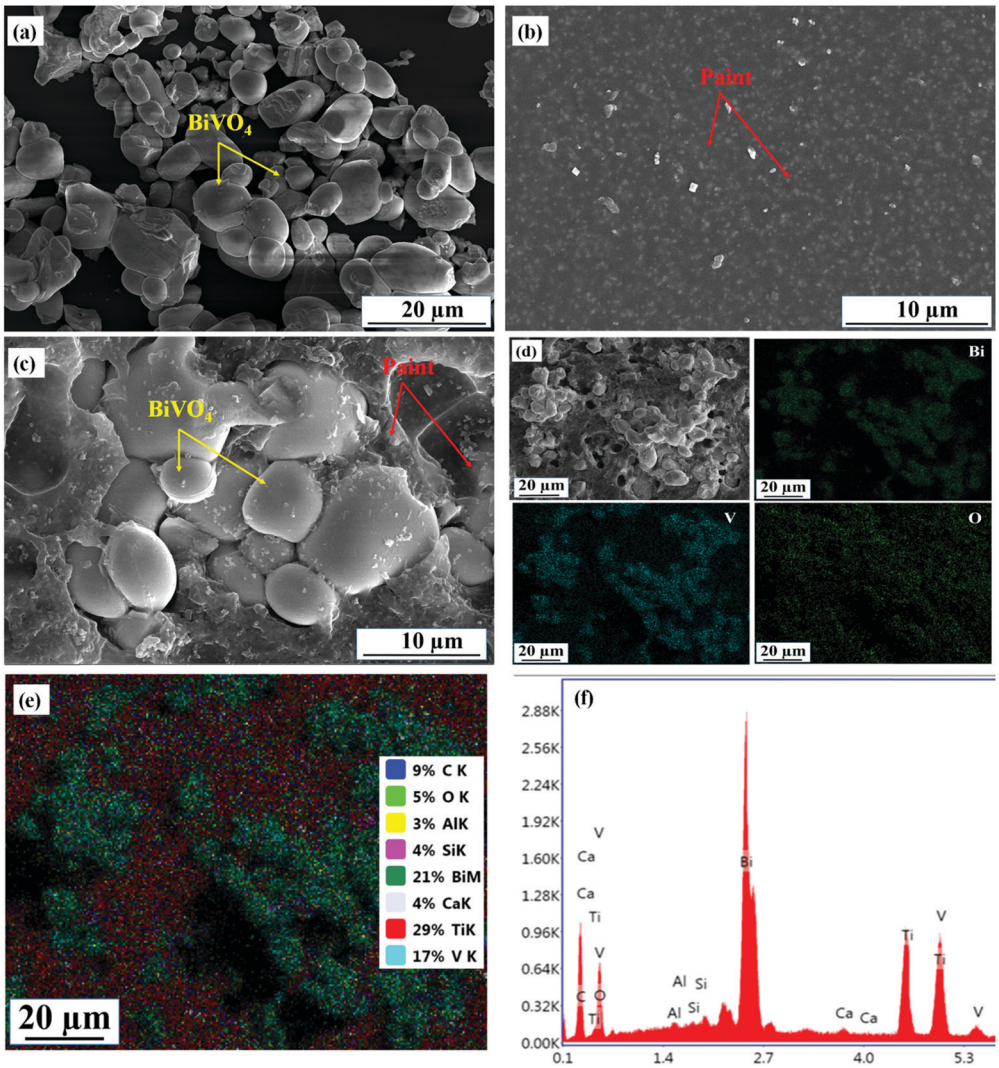

Fig. 2 SEM micrographs of (a) BiV, (b) paint, and (c) 40BiV-paint; (d and e) EDS color mapping of 40BiV-paint; and (f) EDS spectrum obtained for the 40BiV-paint sample.

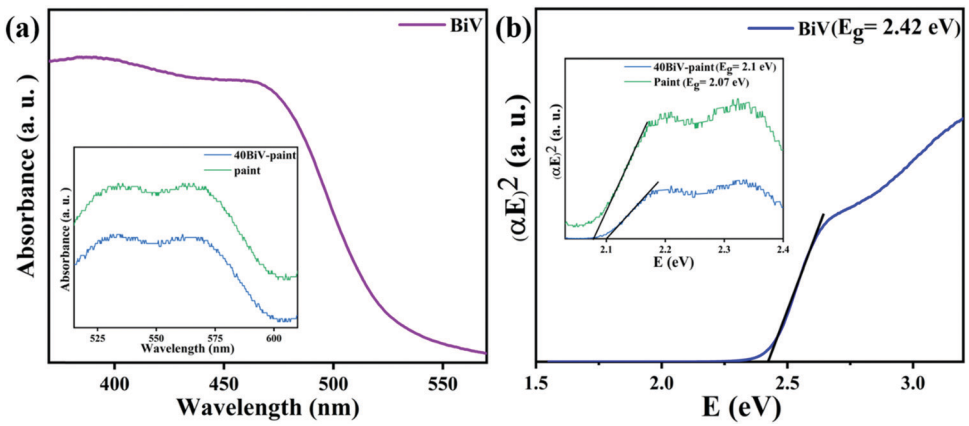

Fig. 3 (a) UV-vis absorption spectrum of BiV powder (inset graph shows the absorption edge of 40BiV-paint and paint) and (b) bandgap of BiV using Tauc plots (inset graph shows the bandgap of 40BiV-paint and paint).

like hydroxyl radicals ($^{\bullet}OH$), holes (h^{+}) and superoxide radicals ($^{\bullet}O_2^{-}$), respectively.[81] Fig. 6(d) shows that the BQ scavenger that scavenges $O_2^{\bullet-}$ radicals has a major influence on the photocatalytic dye degradation efficiency.[81,82] This confirms $O_2^{\bullet-}$

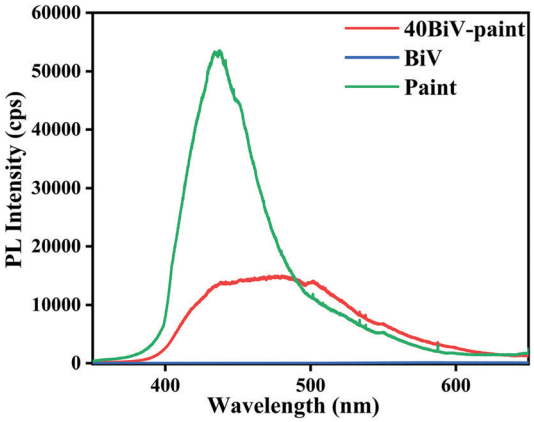

Fig. 4 Photoluminescence spectra of 40BiV-paint, BiV, and paint.

radicals as the major active and dominant species in the commencing photocatalytic dye degradation experiment.

Fig. 7(a) shows the $-\ln\left(\frac{C}{C_o}\right)$ *vs.* time plots attained during the photocatalytic experiment with different MB dye concentrations using the 40BiV-paint sample. The MB dye degradation reaction during photocatalysis is in accordance with the pseudo first-order kinetics as given in eqn (3):[83–85]

$$\ln\frac{C}{C_o} = -kt \quad (3)$$

where '*k*' represents the kinetic rate constant, which is calculated from the slope of the $\ln\frac{C}{C_o}$ *vs.* time '*t*' linear plot. The 40BiV-paint sample attains the largest *k* value of 0.00524 min^{-1} in 5 mg L^{-1} dye and showed a decline in the *k* value as the MB dye concentration is elevated. Fig. 7(b) shows the plots of kinetic rate constant '*k*' *vs.* different dye concentrations (5, 10, and 12.5 mg L^{-1}).

For conducting the germination index test, 3 vials each containing 10 seeds of *Vigna radiata* were taken. The vials were sprinkled everyday with 0.5 ml of treated, untreated, and DI water. Fig. 8(a–c) show the growth of seeds using dye water collected before photocatalysis, treated water collected after 4 h of photocatalysis, and distilled water. According to the results, 5 mg L^{-1} untreated dye water causes more hindrance for the seed growth as compared to the DI and treated water. Although the seed growth using treated water lies in the non-toxic approach, precaution still needs to be taken in the case of edible plants owing to the associated harmful adverse effects.[74] A better suggestion would be to utilize the treated waste water for irrigating parks and playground which would surely decrease the burden on natural water need.[86] Fig. 8(d) displays the results of the phytotoxicity test. For a better understanding of the compounds on the basis of GI values, a major classification has been made: high phytotoxicity (GI < 50%), moderate phytotoxicity (50% < GI < 80%), and the absence of phytotoxicity (GI > 80%). This toxicity level classification adheres to the criteria as suggested by Emino *et al.*[87] and Zucconi *et al.*[75] The results suggest that untreated dye water falls in the level of high toxicity, while treated water after the photocatalysis experiment falls in moderate phytotoxicity.[75] For the GI test treated water after the photocatalysis experiment were taken in use. According to the results, untreated dye water lies in high toxicity, while photocatalytically treated water lies at the level of moderate phytotoxicity. Treated water used for the GI test is the same dye water that attained 58% dye degradation efficiency after the photocatalysis experiment. Thus, further improvement in the efficiency to 100% clean wastewater is also attainable by an increase in catalyst load, an increase in degradation time duration and a decrease in dye concentration.[88,89]

Fig. 9 presents the schematic mechanism of the BiV-paint sample undergoing MB dye degradation during the photocatalysis experiment. The inset of Fig. 9 shows the optical transition of m-$BiVO_4$. As visible light falls on $BiVO_4$, electron–hole pairs are generated on the $BiVO_4$ surface. This causes the excitation of VB electrons to the CB while leaving holes in the VB. There is an optical transition of m-$BiVO_4$ from Bi 6s–O 2p hybrid orbitals to vacant V 3d orbitals which results in a reduced bandgap of 2.4 eV. Coupling among V 3d, O 2p, and Bi 6s causes a lowering of the conduction band minimum. These interactions form symmetric electron and hole masses and

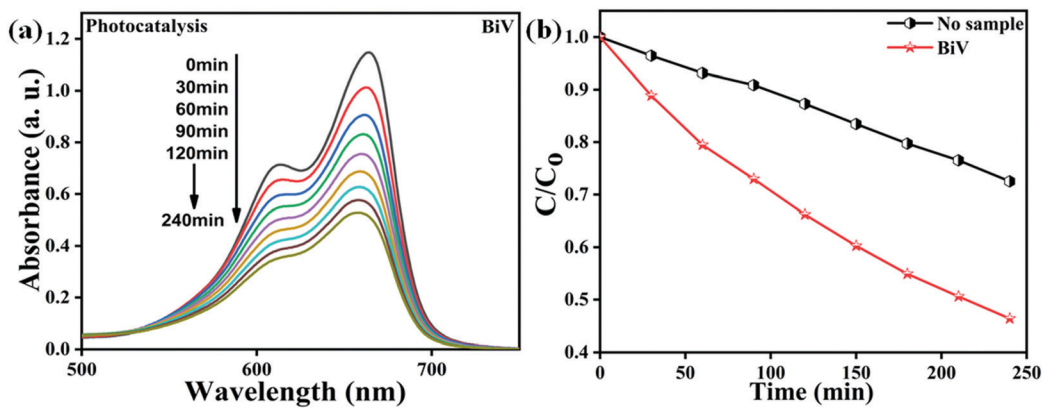

Fig. 5 (a) The acquired absorption spectra from the photocatalysis using BiV powders and (b) $\frac{C}{C_o}$ *vs.* time plots acquired from the photocatalysis with and without any sample use.

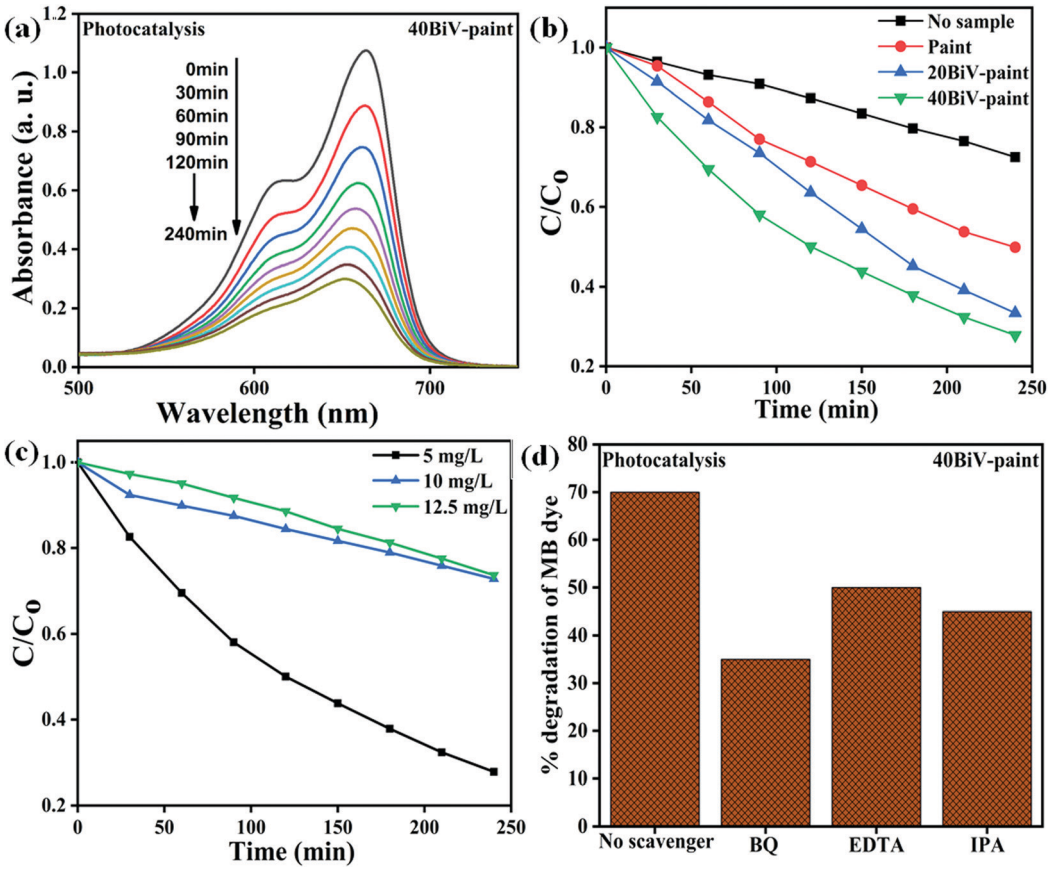

Fig. 6 (a) Absorption spectra acquired from the photocatalysis using the 40BiV-paint sample, (b) $\frac{C}{C_o}$ *vs.* time plots acquired from photocatalysis with and without any sample use, (c) $\frac{C}{C_o}$ *vs.* time plots acquired from photocatalysis using the 40BiV-paint sample at different MB dye concentrations (5, 10, and 12.5 mg L^{-1}), and (d) effect of different scavengers on MB dye degradation efficiency acquired from the photocatalysis experiment using the 40BiV-paint sample.

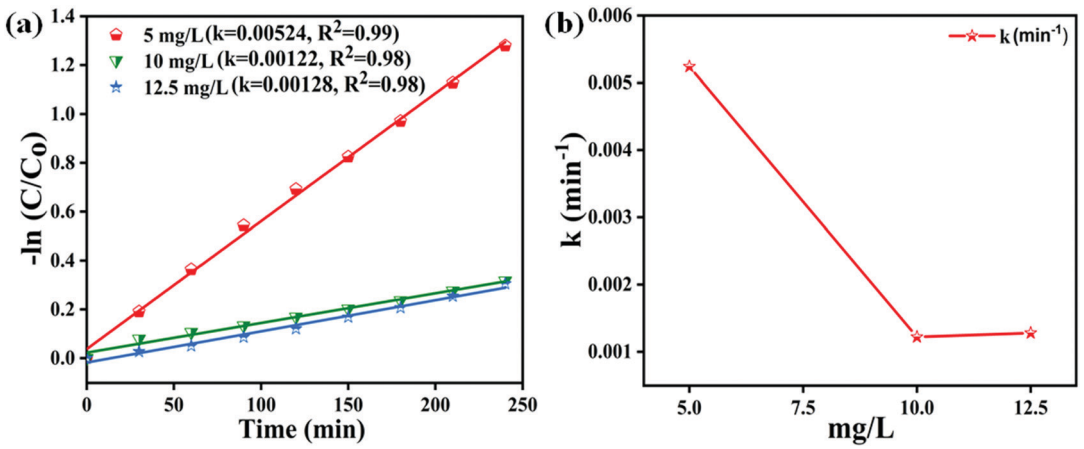

Fig. 7 (a) $-\ln\left(\frac{C}{C_o}\right)$ *vs.* time plots for various MB dye concentrations (mg L^{-1}) and (b) plots of kinetic rate constant '*k*' *vs.* varied dye concentrations during photocatalysis.

thus assist in efficient toxic carrier separation.[38] The generated holes cause oxidation of the adsorbed water producing hydroxyl radicals ($OH^{\bullet}$), while the generated electrons react with the adsorbed oxygen (O_2) producing superoxide radicals ($O_2^{\bullet-}$). These ($O_2^{\bullet-}$ and $OH^{\bullet}$) radicals are further called as reactive oxygen species (ROS) which lead to MB dye degradation to

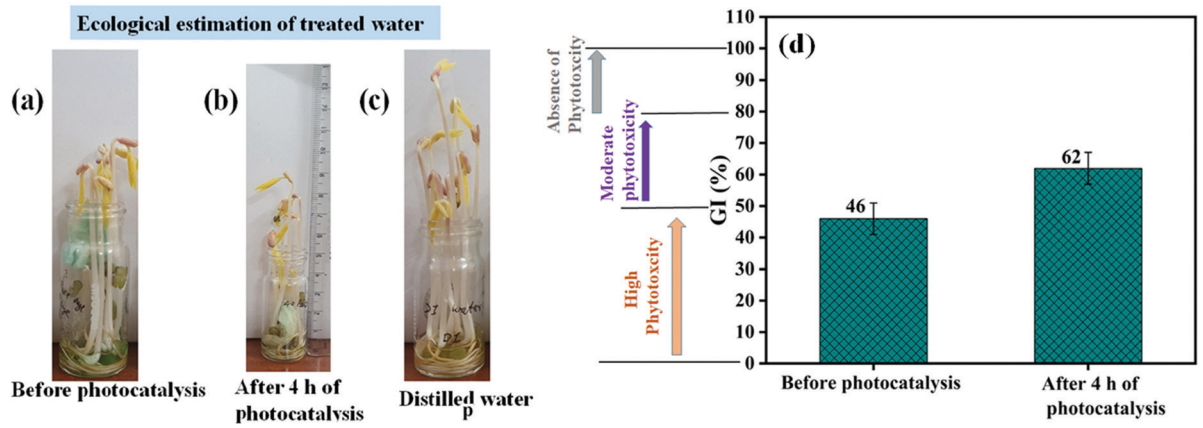

Fig. 8 The impact of the MB dye on the growth of the *Vigna radiata* seeds explored for 7 days; the treatment is done using (a) 5 mg L^{-1} MB dye, (b) treated wastewater and (c) distilled water; (d) germination index test done on two samples after 0 and 4 h of photocatalysis.

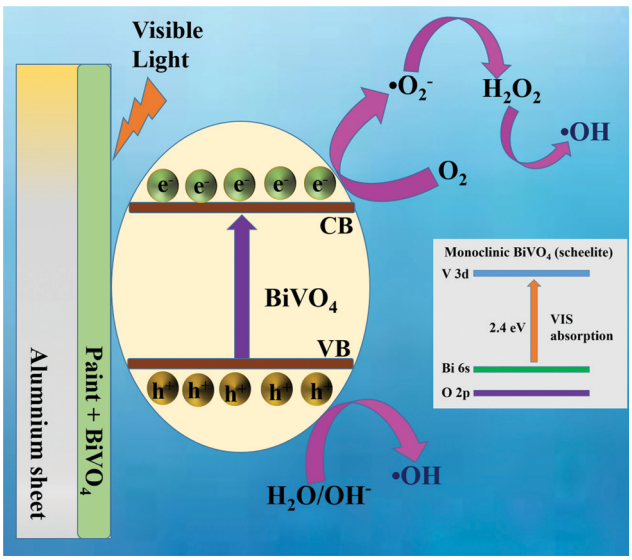

Fig. 9 Schematic mechanism for photocatalytic MB dye degradation using the BiV-paint sample.

harmless products.[90–92] Thus, the BiV-paint sample demonstrates photocatalytic activity.

4. Conclusions

The dye degradation capability of bismuth vanadate mixed in paint during the photocatalysis experiment in visible light was studied. As the content of $BiVO_4$ in the $BiVO_4$–paint sample increases, there is an increase in the dye degradation efficiency. The 40 wt%-$BiVO_4$–paint sample exhibited an ~72% dye degradation efficiency as compared to the 0 wt%-$BiVO_4$–paint sample (~27%) in a duration of 240 min of the photocatalysis experiment. The photocatalytic MB dye degradation is in accordance with the pseudo-first-order kinetics with 0.00524 min^{-1} as the largest k value attained. Photocatalytically treated water after the photocatalysis experiment falls in the moderate phytotoxicity level. The usage of paint coated substrates for wastewater remediation through the photocatalysis experiment using visible light irradiation would be both economical as well as free from separation and filtration processes to recover the catalyst.

Data availability

All data are available within this manuscript.

Conflicts of interest

The authors proclaim of having no conflicts of interest.

References

1 M. Bodzek and M. Rajca, Photocatalysis in the treatment and disinfection of water. Part I. Theoretical backgrounds/ Fotokataliza w oczyszczaniu i dezynfekcji wody część i. podstawy teoretyczne, *Ecol. Chem. Eng. S*, 2012, **19**(4), 489–512.
2 S. S. Shinde, C. H. Bhosale and K. Y. Rajpure, Photocatalytic activity of sea water using TiO_2 catalyst under solar light, *J. Photochem. Photobiol., B*, 2011, **103**(2), 111–117.
3 F. Li, C. Yang, Q. Li, W. Cao and T. Li, The pH-controlled morphology transition of $BiVO_4$ photocatalysts from microparticles to hollow microspheres, *Mater. Lett.*, 2015, **145**, 52–55.
4 C. P. Sajan, S. Wageh, A. Al-Ghamdi, J. Yu and S. Cao, TiO_2 nanosheets with exposed {001} facets for photocatalytic applications, *Nano Res.*, 2016, **9**(1), 3–27.
5 V. P. Singh and R. Vaish, Cement-based diesel exhaust emission soot coatings for the removal of organic pollutants from water, *Constr. Build. Mater.*, 2020, **234**, 117377.
6 T. Robinson, G. McMullan, R. Marchant and P. Nigam, Remediation of dyes in textile effluent: a critical review on

current treatment technologies with a proposed alternative, *Bioresour. Technol.*, 2001, **77**(3), 247–255.

7 S. Ye, M. Yan, X. Tan, J. Liang, G. Zeng and H. Wu, *et al.*, Facile assembled biochar-based nanocomposite with improved graphitization for efficient photocatalytic activity driven by visible light, *Appl. Catal., B*, 2019, **250**, 78–88.

8 S. Ye, G. Zeng, H. Wu, J. Liang, C. Zhang and J. Dai, *et al.*, The effects of activated biochar addition on remediation efficiency of co-composting with contaminated wetland soil, *Resour., Conserv. Recycl.*, 2019, **140**, 278–285.

9 S. Ye, G. Zeng, H. Wu, C. Zhang, J. Dai and J. Liang, *et al.*, Biological technologies for the remediation of co-contaminated soil, *Crit. Rev. Biotechnol.*, 2017, **37**(8), 1062–1076.

10 S. Ye, G. Zeng, H. Wu, C. Zhang, J. Liang and J. Dai, *et al.*, Co-occurrence and interactions of pollutants, and their impacts on soil remediation—a review, *Crit. Rev. Environ. Sci. Technol.*, 2017, **47**(16), 1528–1553.

11 K. Rajeshwar, M. E. Osugi, W. Chanmanee, C. R. Chenthamarakshan, M. V.-B. Zanoni and P. Kajitvichyanukul, *et al.*, Heterogeneous photocatalytic treatment of organic dyes in air and aqueous media, *J. Photochem. Photobiol., C*, 2008, **9**(4), 171–192.

12 V. K. Gupta, I. Ali, T. A. Saleh, A. Nayak and S. Agarwal, Chemical treatment technologies for waste-water recycling—an overview, *RSC Adv.*, 2012, **2**(16), 6380–6388.

13 H. M. Coleman, B. R. Eggins, J. A. Byrne, F. L. Palmer and E. King, Photocatalytic degradation of 17-β-oestradiol on immobilised TiO_2, *Appl. Catal., B*, 2000, **24**(1), L1–L5.

14 S. Esplugas, D. M. Bila, L. G.-T. Krause and M. Dezotti, Ozonation and advanced oxidation technologies to remove endocrine disrupting chemicals (EDCs) and pharmaceuticals and personal care products (PPCPs) in water effluents, *J. Hazard. Mater.*, 2007, **149**(3), 631–642.

15 P. R. Gogate and A. B. Pandit, A review of imperative technologies for wastewater treatment II: hybrid methods, *Adv. Environ. Res.*, 2004, **8**(3–4), 553–597.

16 H. K. Moo-Young, Pulp and paper effluent management, *Water Environ. Res.*, 2007, **79**(10), 1733–1741.

17 D. S. Bhatkhande, V. G. Pangarkar and A. A. C. M. Beenackers, Photocatalytic degradation for environmental applications–a review, *J. Chem. Technol. Biotechnol.*, 2002, **77**(1), 102–116.

18 W. Ma, J. Li, X. Tao, J. He, Y. Xu and J. C. Yu, *et al.*, efficient degradation of organic pollutants by using dioxygen activated by resin-exchanged iron(II) bipyridine under visible irradiation, *Angew. Chem.*, 2003, **115**(9), 1059–1062.

19 M. Kumar, M. N.-M. Ansari, I. Boukhris, M. S. Al-Buriahi, Z. A. Alrowaili and N. Alfryyan, *et al.*, Sonophotocatalytic Dye Degradation Using rGO-$BiVO_4$ Composites, *Glob Challenges*, 2022, 2100132.

20 T. Banerjee and A. Mukherjee, Overall water splitting under visible light irradiation using nanoparticulate RuO_2 loaded Cu_2O powder as photocatalyst, *Energy Procedia*, 2014, **54**, 221–227.

21 C. Regmi, B. Joshi, S. K. Ray, G. Gyawali and R. P. Pandey, Understanding mechanism of photocatalytic microbial decontamination of environmental wastewater, *Front. Chem.*, 2018, **6**, 33.

22 A. R. Khataee and M. B. Kasiri, Photocatalytic degradation of organic dyes in the presence of nanostructured titanium dioxide: Influence of the chemical structure of dyes, *J. Mol. Catal. A: Chem.*, 2010, **328**(1–2), 8–26.

23 Y. Guo, L. Chen, F. Ma, S. Zhang, Y. Yang and X. Yuan, *et al.*, Efficient degradation of tetrabromobisphenol A by hetero-structured Ag/$Bi_5Nb_3O_{15}$ material under the simulated sunlight irradiation, *J. Hazard. Mater.*, 2011, **189**(1–2), 614–618.

24 S. Janitabar-Darzi and A. R. Mahjoub, Investigation of phase transformations and photocatalytic properties of sol–gel prepared nanostructured ZnO/TiO_2 composites, *J. Alloys Compd.*, 2009, **486**(1–2), 805–808.

25 S. Chakrabarti and B. K. Dutta, Photocatalytic degradation of model textile dyes in wastewater using ZnO as semiconductor catalyst, *J. Hazard. Mater.*, 2004, **112**(3), 269–278.

26 H. Golmojdeh and M. A. Zanjanchi, A facile approach for synthesis of $BiVO_4$ nano-particles possessing high surface area and various morphologies, *Cryst. Res. Technol.*, 2012, **47**(9), 1014–1025.

27 L. Järup, Hazards of heavy metal contamination, *Br. Med. Bull.*, 2003, **68**(1), 167–182.

28 A. Kołodziejczak-Radzimska and T. Jesionowski, Zinc oxide—from synthesis to application: a review, *Materials*, 2014, **7**(4), 2833–2881.

29 X. Liu, F. Wang and Q. Wang, Nanostructure-based WO_3 photoanodes for photoelectrochemical water splitting, *Phys. Chem. Chem. Phys.*, 2012, **14**(22), 7894–7911.

30 A. Kudo, K. Omori and H. A. Kato, Phosphate Doping Into Monoclinic $BiVO_4$ for Enhanced Photoelectrochemiczd Water Oxidation Activity, *J. Am. Chem. Soc.*, 1999, **121**(49), 11459–11467.

31 M. Guo, Y. Wang, Q. He, W. Wang, W. Wang and Z. Fu, *et al.*, Enhanced photocatalytic activity of S-doped $BiVO_4$ photocatalysts, *RSC Adv.*, 2015, **5**, 58633–58639.

32 Y. Hu, J. Fan, C. Pu, H. Li, E. Liu and X. Hu, Facile synthesis of double cone-shaped $Ag_4V_2O_7$/$BiVO_4$ nanocomposites with enhanced visible light photocatalytic activity for environmental purification, *J. Photochem. Photobiol., A*, 2017, **337**, 172–183.

33 G. Singh, M. Kumar and R. Vaish, Promising multicatalytic and adsorption capabilities in V_2O_5/$BiVO_4$ composite pellets for water-cleaning application, *Surf. Interfaces*, 2021, **23**(November 2020), 100924, DOI: **10.1016/j.surfin.2021.100924**, available from: .

34 M. Kumar, G. Singh and R. Vaish, A reduced graphene oxide/bismuth vanadate composite as an efficient piezocatalyst for degradation of organic dye, *Mater. Adv.*, 2021, **2**(12), 4093–4101.

35 J. K. Cooper, S. Gul, F. M. Toma, L. Chen, Y.-S. Liu and J. Guo, *et al.*, Indirect bandgap and optical properties of monoclinic bismuth vanadate, *J. Phys. Chem. C*, 2015, **119**(6), 2969–2974.

36 Y. Hermans, A. Klein, K. Ellmer, R. van de Krol, T. Toupance and W. Jaegermann, Energy-band alignment of $BiVO_4$ from

photoelectron spectroscopy of solid-state interfaces, *J. Phys. Chem. C*, 2018, **122**(36), 20861–20870.

37 J. K. Cooper, S. Gul, F. M. Toma, L. Chen, P. A. Glans and J. Guo, *et al.*, Electronic structure of monoclinic $BiVO_4$, *Chem. Mater.*, 2014, **26**(18), 5365–5373.

38 A. Walsh, Y. Yan, M. N. Huda, M. M. Al-Jassim and S.-H. Wei, Band edge electronic structure of $BiVO_4$: elucidating the role of the Bi s and V d orbitals, *Chem. Mater.*, 2009, **21**(3), 547–551.

39 M. Kumar, R. Vaish and S. ben Ahmed, Piezo-photocatalytic activity of mechanochemically synthesized $BiVO_4$ for dye cleaning, *J. Am. Ceram. Soc.*, 2022, DOI: **10.1111/jace.18233**.

40 Q. Luo, L. Zhang, X. Chen, O. K. Tan and K. C. Leong, Mechanochemically synthesized m-$BiVO_4$ nanoparticles for visible light photocatalysis, *RSC Adv.*, 2016, **6**(19), 15796–15802.

41 M. Han, X. Chen, T. Sun, O. K. Tan and M. S. Tse, Synthesis of mono-dispersed m-$BiVO_4$ octahedral nano-crystals with enhanced visible light photocatalytic properties, *CrystEngComm*, 2011, **13**(22), 6674–6679.

42 M. Hofmann, M. Rainer, S. Schulze, M. Hietschold and M. Mehring, Nonaqueous Synthesis of a Bismuth Vanadate Photocatalyst By Using Microwave Heating: Photooxidation versus Photosensitized Decomposition in Visible-Light-Driven Photocatalysis, *ChemCatChem*, 2015, **7**(8), 1357–1365.

43 M. C. Neves and T. Trindade, Chemical bath deposition of $BiVO_4$, *Thin Solid Films*, 2002, **406**(1–2), 93–97.

44 I. Hincapié, A. Caballero-Guzman, D. Hiltbrunner and B. Nowack, Use of engineered nanomaterials in the construction industry with specific emphasis on paints and their flows in construction and demolition waste in Switzerland, *Waste Manage.*, 2015, **43**, 398–406.

45 P. Van Broekhuizen, F. van Broekhuizen, R. Cornelissen and L. Reijnders, Use of nanomaterials in the European construction industry and some occupational health aspects thereof, *J. Nanopart. Res.*, 2011, **13**(2), 447–462.

46 J. Teizer, M. Venugopal, W. Teizer and J. Felkl, Nanotechnology and its impact on construction: bridging the gap between researchers and industry professionals, *J. Constr. Eng. Manag.*, 2012, **138**(5), 594–604.

47 J. Lee, S. Mahendra and P. J.-J. Alvarez, Nanomaterials in the construction industry: a review of their applications and environmental health and safety considerations, *ACS Nano*, 2010, **4**(7), 3580–3590.

48 J.-P. Kaiser, S. Zuin and P. Wick, Is nanotechnology revolutionizing the paint and lacquer industry? A critical opinion, *Sci. Total Environ.*, 2013, **442**, 282–289.

49 M. J. Hanus and A. T. Harris, Nanotechnology innovations for the construction industry, *Prog. Mater. Sci.*, 2013, **58**(7), 1056–1102.

50 M. Saxena and L. K. Dhimole, Utilization and value addition of copper tailing as an extender for development of paints, *J. Hazard. Mater.*, 2006, **129**(1–3), 50–57.

51 J. Pospıšil and S. Nešpurek, Photostabilization of coatings. Mechanisms and performance, *Prog. Polym. Sci.*, 2000, **25**(9), 1261–1335.

52 H. Ye, L. Zhu, W. Li, G. Jiang, H. Liu and H. Chen, Anchoring CeO_2 nanoparticles on monodispersed SiO2 spheres to construct hydrophobic polymer coating with enhanced UV absorption ability, *Chem. Eng. J.*, 2017, **321**, 268–276.

53 Q. Yu, X. Xu, C. Wang, Y. Ma, D. Hui and Z. Zhou, Remarkably improvement in antibacterial activity by synergistic effect in n-Cu@T-ZnO nanocomposites, *Composites, Part B*, 2017, **110**, 32–38.

54 A. Zhang, B. Mu, Z. Luo and A. Wang, Bright blue halloysite/$CoAl_2O_4$ hybrid pigments: preparation, characterization and application in water-based painting, *Dyes Pigm.*, 2017, **139**, 473–481.

55 E. Huajaikaew, T. Piroonpan, K. Booncharoen and W. Pasanphan, Comb-like poly(dodecyl methacrylate) modified SiO_2 nanoparticles as nanohybrid coatings: Electron beam grafting and tuning superhydrophobic/water-repellent surface studies, *Prog. Org. Coat.*, 2022, **163**, 106658.

56 D. Truffier-Boutry, B. Fiorentino, V. Bartolomei, R. Soulas, O. Sicardy and A. Benayad, *et al.*, Characterization of photocatalytic paints: a relationship between the photocatalytic properties–release of nanoparticles and volatile organic compounds, *Environ. Sci.: Nano*, 2017, **4**(10), 1998–2009.

57 A. Gandolfo, L. Rouyer, H. Wortham and S. Gligorovski, The influence of wall temperature on NO_2 removal and HONO levels released by indoor photocatalytic paints, *Appl. Catal., B*, 2017, **209**, 429–436.

58 A. L. da Silva, D. N.-F. Muche, S. Dey, D. Hotza and R. H.-R. Castro, Photocatalytic Nb_2O_5-doped TiO_2 nanoparticles for glazed ceramic tiles, *Ceram. Int.*, 2016, **42**(4), 5113–5122.

59 C. Toro, B. T. Jobson, L. Haselbach, S. Shen and S. H. Chung, Photoactive roadways: Determination of CO, NO and VOC uptake coefficients and photolabile side product yields on TiO_2 treated asphalt and concrete, *Atmos. Environ.*, 2016, **139**, 37–45.

60 E. Boonen and A. Beeldens, Recent photocatalytic applications for air purification in Belgium, *Coatings*, 2014, **4**(3), 553–573.

61 S. M. Amorim, J. Suave, L. Andrade, A. M. Mendes, H. J. Jose and R. F. P. M. Moreira, Towards an efficient and durable self-cleaning acrylic paint containing mesoporous TiO_2 microspheres, *Prog. Org. Coat.*, 2018, **118**, 48–56.

62 R. E. Day, The role of titanium dioxide pigments in the degradation and stabilisation of polymers in the plastics industry, *Polym. Degrad. Stab.*, 1990, **29**(1), 73–92.

63 M. Baudys, J. Krýsa and A. Mills, Smart inks as photocatalytic activity indicators of self-cleaning paints, *Catal. Today*, 2017, **280**, 8–13.

64 M. T. Islam, A. Dominguez, R. S. Turley, H. Kim, K. A. Sultana and M. A.-I. Shuvo, *et al.*, Development of photocatalytic paint based on TiO_2 and photopolymer resin for the degradation of organic pollutants in water, *Sci. Total Environ.*, 2020, **704**, 135406.

65 A. Bonnefond, E. González, J. M. Asua, J. R. Leiza, E. Ieva and G. Brinati, *et al.*, Stable photocatalytic paints prepared

from hybrid core-shell fluorinated/acrylic/TiO_2 waterborne dispersions, *Crystals*, 2016, **6**(10), 136.

66 A. Bonnefond, E. González, J. M. Asua, J. R. Leiza, J. Kiwi and C. Pulgarin, *et al.*, New evidence for hybrid acrylic/TiO_2 films inducing bacterial inactivation under low intensity simulated sunlight, *Colloids Surf., B*, 2015, **135**, 1–7.

67 S. M. D. Amorim, J. C. Sapatieri, D. E. Moritz, M. D. Domenico, L. A. D. C. Laqua, C. D. Moura-Nickel and R. D. F. P. M. Moreira, Antifungal and photocatalytic activity of smart paint containing porous microspheres of TiO_2, *Mater. Res.*, 2020, **22**(6), DOI: 10.1590/1980-5373-MR-2019-0470.

68 L. M. Farrier and S. L. Szaruga, Sample preparation and characterization of artificially aged aircraft coatings for microstructural analysis, *Mater. Charact.*, 2005, **55**(3), 179–189.

69 Y. Zhu, L. Zhang, L. Wang, R. Tan and L. Cao, Interface diffusion and reaction between TiO_2 film photocatalyst and aluminium alloy substrate, *Surf. Interface Anal.*, 2001, **32**(1), 218–223.

70 N. Hassan, S. Lu, W. Xu, H. Ge and A. Sultana, Fabrication of stable superhydrophobic bismuth material on the aluminum substrate with high photocatalytic activity, *J. Nanopart. Res.*, 2021, **23**(4), 1–15.

71 J.-G. Nam, E.-S. Lee, W.-C. Jung, Y.-J. Park, B.-H. Sohn and S.-C. Park, *et al.*, Photovoltaic enhancement of dye-sensitized solar cell prepared from [TiO_2/ethyl cellulose/terpineol] paste employing TRITON^{TM} X-based surfactant with carboxylic acid group in the oxyethylene chain end, *Mater. Chem. Phys.*, 2009, **116**(1), 46–51.

72 M. Meinert and G. Reiss, Electronic structure and optical band gap determination of $NiFe_2O_4$, *J. Phys.: Condens. Matter*, 2014, **26**(11), 115503.

73 Z. Shao, X. Meng, H. Lai, D. Zhang, X. Pu and C. Su, *et al.*, Coralline-like Ni2P decorated novel tetrapod-bundle $Cd_{0.9}Zn_{0.1}$SZB/WZ homojunctions for highly efficient visible-light photocatalytic hydrogen evolution, *Chin. J. Catal.*, 2021, **42**(3), 439–449.

74 A. Priac, P.-M. Badot and G. Crini, Treated wastewater phytotoxicity assessment using Lactuca sativa: focus on germination and root elongation test parameters, *C. R. Biol.*, 2017, **340**(3), 188–194.

75 H. Zeghioud, N. Khellaf, A. Amrane, H. Djelal, M. Bouhelassa and A. A. Assadi, *et al.*, Combining photocatalytic process and biological treatment for Reactive Green 12 degradation: optimization, mineralization, and phytotoxicity with seed germination, *Environ. Sci. Pollut. Res.*, 2021, **28**(10), 12490–12499.

76 E. Ozel, G. Unluturk and S. Turan, Production of brown pigments for porcelain insulator applications, *J. Eur. Ceram. Soc.*, 2006, **26**(4–5), 735–740.

77 Q. I. Zwane, S. Moeno and L. N. Dlamini, A multiphase $BiVO_4$ with the potential of being an environmental photocatalyst, *Appl. Nanosci.*, 2019, **9**(4), 539–555.

78 K. Anwar, F. K. Naqvi and S. Beg, Synthesis of tetragonally stabilized lanthanum doped bismuth vanadium oxide nanoparticles and its enhanced visible light induced photocatalytic performance, *Phase Transitions*, 2022, **95**(1), 64–79.

79 M. M. Sajid, S. B. Khan, N. A. Shad and N. Amin, Synthesis of $Zn_3(VO_4)_2$/$BiVO_4$ heterojunction composite for the photocatalytic degradation of methylene blue organic dye and electrochemical detection of H_2O_2, *RSC Adv.*, 2018, **8**(62), 35403–35412.

80 P. Praus, J. Lang, A. Martaus, L. Svoboda, V. Matějka and M. Kormunda, *et al.*, Composites of $BiVO_4$ and g-C3N4: synthesis, properties and photocatalytic decomposition of Azo Dye AO7 and nitrous oxide, *J. Inorg. Organomet. Polym. Mater.*, 2019, **29**(4), 1219–1234.

81 U. Alam, A. Khan, D. Ali, D. Bahnemann and M. Muneer, Comparative photocatalytic activity of sol-gel derived rare earth metal (La, Nd, Sm and Dy)-doped ZnO photocatalysts for degradation of dyes, *RSC Adv.*, 2018, **8**(31), 17582–17594.

82 J. H. Shah, M. Fiaz, M. Athar, J. Ali, M. Rubab, R. Mehmood and R. Djellabi, Facile synthesis of N/B-double-doped Mn_2O_3 and WO_3 nanoparticles for dye degradation under visible light, *Environ. Technol.*, 2019, **41**(18), 2372–2381.

83 E. Prabakaran and K. Pillay, Synthesis of N-doped ZnO nanoparticles with cabbage morphology as a catalyst for the efficient photocatalytic degradation of methylene blue under UV and visible light, *RSC Adv.*, 2019, **9**(13), 7509–7535.

84 B. Vellaichamy and P. Periakaruppan, Ag nanoshell catalyzed dedying of industrial effluents, *RSC Adv.*, 2016, **6**(38), 31653–31660.

85 C. Yang, W. Dong, G. Cui, Y. Zhao, X. Shi and X. Xia, *et al.*, Highly efficient photocatalytic degradation of methylene blue by P2ABSA-modified TiO_2 nanocomposite due to the photosensitization synergetic effect of TiO_2 and P2ABSA, *RSC Adv.*, 2017, **7**(38), 23699–23708.

86 A. Singh, A. Bhati, P. Khare, K. M. Tripathi and S. K. Sonkar, Soluble graphene nanosheets for the sunlight-induced photodegradation of the mixture of dyes and its environmental assessment, *Sci. Rep.*, 2019, **9**(1), 1–12.

87 E. R. Emino and P. R. Warman, Biological assay for compost quality, *Compost Sci. Util.*, 2004, **12**(4), 342–348.

88 S. Tu, Y. Guo, Y. Zhang, C. Hu, T. Zhang and T. Ma, *et al.*, Piezocatalysis and Piezo-Photocatalysis: Catalysts Classification and Modification Strategy, Reaction Mechanism, and Practical Application, *Adv. Funct. Mater.*, 2020, **30**(48), 2005158.

89 A. Kumar and G. Pandey, A review on the factors affecting the photocatalytic degradation of hazardous materials, *Mater. Sci. Eng.*, 2017, **1**(3), 1–10.

90 Y. Zhang, Z. Yang, R. Li, H. Geng and C. Dong, Investigation of fine chalk dust particles' chemical compositions and toxicities on alveolar macrophages in vitro, *Chemosphere*, 2015, **120**, 500–506.

91 H. Lei, H. Zhang, Y. Zou, X. Dong, Y. Jia and F. Wang, Synergetic photocatalysis/piezocatalysis of bismuth oxybromide for degradation of organic pollutants, *J. Alloys Compd.*, 2019, **809**, 151840.

92 G. Tezcanli-Güyer and N. H. Ince, Individual and combined effects of ultrasound, ozone and UV irradiation: a case study with textile dyes, *Ultrasonics*, 2004, **42**(1–9), 603–609.

